TISSUE ENGINEERING: Part A
Volume 21, Numbers 7 and 8, 2015

DOI: 10.1089/ten.tea.2013.0720

# Enhanced Differentiation and Delivery of Mouse Retinal Progenitor Cells Using a Micropatterned Biodegradable Thin-Film Polycaprolactone Scaffold

Jing Yao, MD,[1,2,*] Chi Wan Ko, MS,[3,4,*] Petr Y. Baranov, MD, PhD,[2] Caio V. Regatieri, MD,[2]
Stephen Redenti, PhD,[5] Budd A. Tucker, PhD,[2] Jason Mighty, BA,[5]
Sarah L. Tao, PhD,[3] and Michael J. Young, PhD[2]

The deterioration of retinal tissue in advanced stages of retinitis pigmentosa and age-related macular degeneration and the lack of signaling cues for laminar regeneration are significant challenges highlighting the need for a tissue engineering approach to retinal repair. In this study, we fabricated a biodegradable thin-film polycaprolactone (PCL) scaffold with varying surface topographies using microfabrication techniques. Mouse retinal progenitor cells (mRPCs) cultured on PCL scaffolds exhibited enhanced potential to differentiate toward a photoreceptor fate in comparison to mRPCs cultured on control substrates, suggesting that PCL scaffolds are promising as substrates to guide differentiation of mRPCs toward a photoreceptor fate *in vitro* before transplantation. When cocultured with the retinal explants of rhodopsin null mice, mRPC/PCL constructs showed increased mRPC integration rates compared to directly applied dissociated mRPCs. Moreover, these mRPC/PCL constructs could be delivered into the subretinal space of rhodopsin null mice with minimal disturbance of the host retina. Whether cocultured with retinal explants or transplanted into the subretinal space, newly integrated mRPCs localized to the outer nuclear layer and expressed appropriate markers of photoreceptor fate. Thus, the PCL scaffold provides a platform to guide differentiation and organized delivery of mRPCs as a practical strategy to repair damaged retina.

## Introduction

Retinitis pigmentosa (RP) and age-related macular degeneration (AMD) are leading causes of irreversible blindness characterized by photoreceptor loss.[1,2] The cell transplantation is a promising strategy to replace the damaged or lost cells.[3–5] However in advanced stages of RP and AMD, deterioration of the retinal microenvironment and the lack of signaling cues to promote proper cell organization and differentiation are some of the main challenges highlighting the need for a tissue engineering approach in the success of retinal regeneration.

Recently, an increasing number of synthetic polymer scaffolds have been investigated in retinal tissue engineering,[6–13] including a thin, biodegradable polycaprolactone (PCL) substrate that can be placed into the subretinal space with minimal physical distortion.[9] Unlike bolus injection, cells cultured on polymer scaffolds possess an inherent structural organization and can be precisely placed for cell delivery. Our previous work showed that delivering mouse retinal progenitor cells (mRPCs) to the subretinal space via polymer scaffolds resulted in a 16-fold increase in cell delivery and 10-fold increase in cell survival, thereby promoting cellular integration.[12] However, the percentage of cells that could differentiate into photoreceptors remained limited. Recent studies suggest that delivery of photoreceptor precursors or photoreceptor-committed cells may facilitate differentiation toward photoreceptors.[4,14–16] Earlier studies of microfabricated PCL scaffolds demonstrated increased cell attachment, organization and higher gene expression of the photoreceptor markers recoverin and rhodopsin in mRPCs,[10] making it possible to differentiate these cells toward photoreceptor-committed cells *in vitro* before transplantation.

In this study, we developed a biodegradable thin-film PCL scaffold using microfabrication techniques and a modified soft-lithographic templating process. Topographies, characterized as ridge-groove or post, were inversely replicated into the thin film with minimal deformation. Our analysis suggests

[1]Department of Ophthalmology, Eye and ENT Hospital, Shanghai Medical School, Fudan University, Shanghai, China.
[2]Department of Ophthalmology, Schepens Eye Research Institute, Massachusetts Eye and Ear, Harvard Medical School, Boston, Massachusetts.
[3]The Charles Stark Draper Laboratory, Inc., Cambridge, Massachusetts.
[4]Department of Mechanical Engineering, Massachusetts Institute of Technology, Cambridge, Massachusetts.
[5]Department of Biological Sciences, Lehman College, City University of New York, Bronx, New York.
*These two authors equally contributed to this work.

that based on unique topographic cues, the structured thin-film PCL scaffold had the potential to guide mRPC differentiation and provide a biodegradable platform to organize and deliver mRPCs to the retinal tissue.

## Materials and Methods

### *Animals*

Adult rhodopsin null ($Rho^{-/-}$) C57Bl6 mice (Peter Humphries; Trinity College) and wild-type C57Bl6 mice (Jackson Laboratory) were used as recipient animals. Postnatal day 0 (P0) green fluorescent protein positive ($GFP^{+}$) C57Bl6 mice (Jackson Laboratory) were used as mRPC donors. All experiments were performed according to the Schepens Eye Research Institute Animal Care and Use Committee and the ARVO Statement for the Use of Animals in Ophthalmic and Vision Research.

### *mRPC isolation and culture*

Eyes from P0 $GFP^{+}$ mice were removed and placed in Hank's balanced salt solution (Invitrogen). Neural retinas were carefully dissected away from the retinal pigment epithelium (RPE). Retinal tissue was minced and digested with 0.1% type 1 collagenase (Sigma) for 20 min at room temperature. Liberated cells were collected through a 100 μm mesh strainer (BD), centrifuged at 1000 rpm for 5 min, and resuspended in neurobasal medium (NB; Invitrogen) containing 20 ng/mL epidermal growth factor (EGF; R&D), 2% B-27 (Invitrogen), 1% N2 (Invitrogen), 100 μg/mL penicillin/streptomycin (Invitrogen), 2 mM L-glutamine (Invitrogen), and 2000 U nystatin (Sigma). Cells were transferred to a six-well plate (BD) and cultured at 37°C in a 5% $CO_2$ incubator. About 0.5 mL of fresh medium was added to each well every 2 days. Primary neurospheres formed within the first 2 weeks in culture. These proliferating cultures were passaged 1:3 every 14 days.

### *Thin-film PCL scaffold fabrication*

A silicon master was fabricated with the inverse pattern of the desired surface topographies: ridge-groove or post. A silicon oxide wafer was spun with S1805 positive photoresist, and then exposed with ultraviolet light through a chrome mask (designed using L-Edit and fabricated by Toppan photomasks) with the designed features. Reactive ion etching was performed with Tetrafluoromethane gas at 130 mTorr to achieve an aspect ratio of 1:1. A modified spin-assisted solvent casting method was used to template the master mold features into PCL. A 0.10 mg/mL PCL solution in dichloromethane was dispensed on the silicon master mold and spin cast at 1500 rpm for 30 s, and then heated in an oven at 70°C for 15 min. The PCL thin film was lifted off the wafer by submersion in deionized water. The scaffolds were dried and subjected to oxygen plasma treatment (200 W, 270 mTorr, 30 s) to increase surface hydrophilicity. Smooth PCL (PCL templated off a nonstructured wafer), glass, and polystyrene were used as controls.

### *PCL scaffold preparation*

PCL scaffolds were cut with a sterile scalpel, incubated in 70% ethanol (Pharmco-AAPER) for 12 h, and rinsed thrice with phosphate-buffered saline (PBS) solution (Sigma) in a 12-well plate (BD). Scaffolds were then submerged in modified NB and incubated at 37°C for 1 h.

### *Cell proliferation on PCL scaffold*

Expansion of mRPCs was analyzed on PCL scaffolds. To establish a standard mRPC population curve, total mRPC green fluorescent protein (GFP) signals were detected in a known population from $5\times10^3$ to $5\times10^5$ cells in 96-well plates ($n=3$) using a Tecan Genios microplate reader (Tecan Group Ltd.). A $1\times1$ mm piece of different topographies of PCL scaffolds was then seeded with $2\times10^5$ mRPCs and cultured for 7 days. Total GFP emissions from mRPCs on each topography were taken at day 1, 3, and 7 under identical conditions ($n=3$). The mRPC/PCL scaffold signals and the standard population curve signals were then correlated to establish cell number on each day. After seeding, a Spot ISA-CE camera (Diagnostic Instruments) attached to a Nikon Eclipse TE800 microscope (Micro Video Instruments, Inc.) was used to visualize cell proliferation across each topography of PCL scaffolds. The composites were also imaged at 10× magnification at day 1, 3, and 7.

### *Cell differentiation on different substrates*

To analyze the differentiation of mRPCs on different substrates, mRPCs were dissociated into single cells in modified NB containing reduced EGF concentration to 1 ng/mL, 2% B-27, 1% N2, 100 μg/mL penicillin/streptomycin, 2 mM L-glutamine, and 2000 U nystatin. One hundred microliters of cell suspension ($8\times10^4$ cells) was seeded onto each $4\times4$ mm piece of PCL scaffold, glass, or polystyrene. Cells were allowed to differentiate for 7 days and the medium was changed every other day. Cells were then collected for scanning electron microscope (SEM), immunocytochemistry (ICC), western blotting, and reverse transcription–polymerase chain reaction (RT-PCR), respectively.

### *Scanning electron microscope*

Cell morphology was examined using SEM at day 3, 5, and 7. Before imaging, each sample was fixed in a solution of 3% glutaraldehyde (Sigma), 0.1 M sucrose (Sigma), and 0.1 M sodium cacodylate (Sigma) buffer for 72 h at room temperature. Following fixation, samples were rinsed in buffer containing 0.1 M sucrose and 0.1 M sodium cacodylate. Samples were then dehydrated in a graded ethanol series. The final 100% ethanol was replaced with hexamethyldisilazane (PolySciences, Inc.) for 10 min and subsequently air-dried for 30 min. Samples were sputter-coated with a 20 nm layer of gold–palladium. SEM imaging was conducted on a Hitachi S-3500N SEM (Hitachi High Technologies America, Inc.) at 5 kV.

### *Immunocytochemistry*

The mRPC/PCL scaffold constructs were fixed in 4% paraformaldehyde (Sigma) for 20 min and then processed for ICC as described below. All samples were rinsed thrice for 5 min each in PBS, blocked in PBS containing 10% goat serum (Invitrogen), 3% bovine serum albumin (BSA; Sigma), and 0.1% Triton-X (Sigma) for 1 h. After rinsing once for 5 min in PBS, samples were incubated with the following primary antibodies in 10% goat serum and 3% BSA

overnight at 4°C in a humidified chamber: crx (1:100; Santa Cruz), recoverin (1:1000; Chemicon), rhodopsin (1:100; Chemicon), s-opsin (1:200; Abcam), protein kinase C (PKC, 1:100; Santa cruz), synaptophysin (1:20; Dako) GFP (1:500; Abcam), and GFP (1:500; Chemicon). Ten percent goat serum and 3% BSA was used as negative control for immunostaining. Sections were subsequently incubated in Cy2 (1:100), Cy3 (1:400), or Cy5 (1:150)-conjugated secondary antibodies (Jackson Immunochem) for 1 h at room temperature. Nuclei were counterstained with 4′,6′-diamidino-2-phenylindole hydrochloride (DAPI) and analyzed using Nikon Eclipse E800 fluorescent microscope (Micro Video Instruments, Inc.) or Leica TCS-SP5 confocal microscope (Leica Microsystems). To control for experimental bias, all staining was performed at the same time using the same staining parameters for each experiment.

### *Western blotting*

For western blotting analyses, cells were homogenized in lysis buffer (50 mM Tris-HCl, pH 8.0, 150 mM NaCl, 1% NP-40, 0.5% sodium deoxycholate, and 0.1% sodium dodecyl sulfate [SDS]) and centrifuged. Supernatants were isolated and protein concentrations were determined using a BCA protein assay (Pierce Chemicals). Equivalent amounts of protein (15 μg) were subjected to SDS–polyacrylamide gel electrophoresis (PAGE; 10% acrylamide), transferred to PVDF membrane (Bio-Rad), and probed with the following antibodies: crx (1:1000), recoverin (1:1000), rhodopsin (1:500), and β-actin (1:5000; Abcam). Blots were cut and reprobed sequentially, visualized with ECL reagents (Thermo Scientific), and exposed to X-ray film (Thermo Scientific). Developed films were subsequently digitized and densitometrically analyzed using the Image J software (NIH image, each substrate was normalized against β-actin). Digital images of western blots were used to make composite figures with Adobe Photoshop® graphics software (Adobe Corp.).

### *Reverse transcription–polymerase chain reaction*

Total RNA was extracted from each sample using the RNeasy mini kit (Qiagen) followed by column treatment with DNase I (Qiagen). cDNA was then synthesized from 1 μg of total RNA using Superscript™ III first-strand synthesis system (Invitrogen). The primers were synthesized commercially (Table 1; Invitrogen). Gene expression was analyzed by amplifying 2 μL of cDNA (1:300 dilution from original samples) in a Peltier Thermal Cycler PTC-200 (Bio-Rad) using Platinum Taq DNA Polymerase (Invitrogen). Amplification of glyceraldehyde phosphate dehydrogenase (GAPDH) served as the internal control. Amplification conditions were 30 s/95°C, 45 s/61°C or 62°C, and 1 min/72°C for 35 cycles. PCR products were resolved on a 2% agarose (Invitrogen) gel alongside a 50 bp DNA ladder (Invitrogen). Gels were visualized and photographed in a UV light box. Figures were subsequently digitized and analyzed using the Image J software (NIH image, each substrate was normalized against GAPDH). Digital images of RT-PCR were used to make composite figures with Adobe Photoshop graphics software.

### *Calcium imaging*

Calcium dynamics were analyzed between mRPCs cultured on PCL scaffolds and glass 7 days after plating. For $Ca^{2+}$ imaging, cells were transferred to 35 mm glass bottom Petri dishes (MatTek), allowed to adhere in Neurobasal at 37°C, and then rinsed with Ringer's solution maintained at 37°C containing NaCl 119 mM, KCl 4.16 mM, CaCl 2.5 mM, MgCl 0.3 mM, MgSO 0.4 mM, $Na_2HPO_4$ 0.5 mM, $NaH_2PO_4$ 0.45 mM, HEPES 20 mM, and glucose 19 mM at pH 7.4. Cells were then incubated in Ringer's solution containing 0.5 mm fura-2 tetra-acetoxymethyl ester (Fura-2; Invitrogen), 10% pluronic F127 (Sigma), and 250 mm sulfinpyrazone (Sigma) for 40 min at 22°C. To monitor calcium change, Fura-2 was excited by alternating 340 and 380 nm light[17] with the use of filter changer, under the control of NES Elements software paired to a Nikon Eclipse Ti

Table 1. List of Primers for Reverse Transcription–Polymerase Chain Reaction

| *Gene* | *Primer sequence (5′-3′)* | *Product size (bp)* |
|---|---|---|
| Mouse crx | F: TCTCTCACCTCAGCCCCTTAT<br>R: ACCCACTGAAATAGGAACTTGGA | 100 |
| Mouse GAPDH | F: AGGTCGGTGTGAACGGATTTG<br>R: TGTAGACCATGTAGTTGAGGTCA | 123 |
| Mouse recoverin | F: ATGGGGAATAGCAAGAGCGG<br>R: GAGTCCGGGAAAAACTTGGAATA | 179 |
| Mouse rhodopsin | F: CCCTTCTCCAACGTCACAGG<br>R: TGAGGAAGTTGATGGGGAAGC | 139 |
| Human β-actin | F: CATGTACGTTGCTATCCAGGC<br>R: CTCCTTAATGTCACGCACGAT | 250 |
| Human recoverin | F: CCTCTACGACGTGGACGGTAA<br>R: GTGTTTTCATCGTCTGGAAGGA | 120 |
| Human rhodopsin | F: GTGCCCTTCTCCAATGCGA<br>R: TGAGGAAGTTGATGGGGAAGC | 202 |
| Human ROM1 | F: TCCCTCCTGTCAGTTCCCTG<br>R: TAGAGCTGCATTCAGACTTGC | 115 |

GAPDH, glyceraldehyde phosphate dehydrogenase; ROM1, rod outer membrane 1.

Microscope (Micro Video Instruments, Inc.) and imaged with a Coolsnap HQ2 camera (Photometrics). A new image (340/380) was obtained every 0.5 s. Background intensity was zero. A 30 μL bolus injection brought the stimulant concentration in the cell bath to 1 mM L-glutamate (Sigma).

### *Human RPC isolation and culture*

Human RPCs were dissociated from human fetal retina at 18 week of gestation and expanded as previously described[18]: cells were plated on fibronectin (Akron)-coated plastic (Nunc) in Ultraculture medium (Lonza) supplemented with 10 ng/mL recombinant human EGF and 20 ng/mL basic fibroblast growth factor (Peprotech). After passaging nine times, human RPCs were plated on fibronectin-coated smooth PCL scaffolds or glass at a density of 20,000 cells per $cm^2$. Cells were cultured for 7 days to induce differentiation. Some cells were collected at day 7 for ICC (recoverin, rhodopsin and rod outer membrane 1 [ROM1; Abcam]). Some cells were collected at day 0, 3, 5, and 7 for RT-PCR.

### *Explant cultures*

The procedure used for retinal explants has been described previously.[8,9,19,20] Briefly, Adult $Rho^{-/-}$ or wild-type mice were euthanized and eyes were enucleated immediately and placed in ice-cold PBS. Neural retinas were carefully dissected away from the RPE, transferred to freshly prepared modified NB and cut into four equal-sized pieces. Each piece of the retina was mounted onto 0.4 μm Millicell®-CM Organotypic porous culture well inserts (BD) with its vitreal surface closest to the filter. Culture well inserts containing explants were placed into six-well plates. Two milliliters of modified NB was added to each culture well. A 7-day mRPC/PCL scaffold construct ($1 \times 1$ mm) was put onto the outer surface (sub-retinal) of each retinal explant, and incubated at 37°C with 5% $CO_2$ for 7 days. One microliter of mRPC suspension of the same passage and number was used as a control.

### *Subretinal transplantation*

Transplantation was performed as previously described.[7–9,12,20] Briefly, mice were prepared under general anesthesia with an intraperitoneal injection of ketamine (5 mg/kg) and xylazine (10 mg/kg), followed by local anesthetization with 0.5% proparacaine (Accutome) and dilation of the pupil with 1% tropicamide (Akorn). The temperature of the mice was maintained at 37°C using a heating pad and heat lamp during surgery. Transplantation was performed under an operating microscope. The 7-day mRPC/PCL scaffold construct was cut into $1.0 \times 0.5$ mm pieces before transplantation. An incision (0.5–1.0 mm) perpendicular to the limbal that was 1.0 mm from the limbal was made in the internal posterior sclera using a Sharpoint 5.0-mm blade scalpel (Fine Science Tools). The mRPC/PCL scaffold construct with mRPCs facing the retina was then inserted through the sclerotomy into the subretinal space using No. 5 Dumont forceps (Fine Science Tools). The optic nerve was not affected during the surgery. After the surgery, the fundus was checked to make sure that the scaffold lied flat in the subretinal space. Hemorrhage and retinal tear were excluded. Mice were allowed to recover, returned to their normal housing and permitted to survive for 3 weeks post-transplantation.

### *Fundus examination*

The location of the mRPC/PCL scaffold construct and the structure of the host retina were examined using retinal camera 50IX (Topcon) and spectral domain optical coherence tomography (SD-OCT; Bioptigen) 1 week after transplantation. The mode of radial volume was used in SD-OCT. Each two-dimensional volume recorded at the diameter of 1.3 mm consisted of 100 B scans and each B scan consisted of 1000 A scans.

### *Histology*

Enucleated eyes and explants were fixed in 4% paraformaldehyde for 12 h, and cryoprotected in 10% sucrose, followed by 30% sucrose for 12 h each at 4°C. Eyes and explants were then embedded in optimal cutting temperature compound (Tissue-Tek), frozen on dry ice, and cryosectioned at 16 μm using a Minotome Plus (Triangle Biomedical Sciences). The procedure for ICC was mentioned above.

### *Cell counting*

Cell counts presented in Figure 2 were performed by counting the total number of immunopositive cells and DAPI in 10 randomly selected microscopic fields taken from three experimental repeats. Cell counts presented in Figure 4 were performed by counting the total number of cells that crossed the host retinal border in 12 randomly selected microscopic fields taken from three experimental samples.

### *Statistical analysis*

Each experiment was repeated at least three times. Where appropriate, data are plotted as mean ± standard error of the mean and significance is noted only if $p < 0.05$, as determined by using one-way ANOVA with Turkey testing for *post hoc* comparisons or Student's *t*-test.

## Results

### *PCL scaffold fabrication*

To increase the ease of cell delivery and reduce the risk of trauma to the retina, the biodegradable PCL scaffold (Fig. 1a–c) was constructed with an average thickness of 5 μm. Surface topographies, including ridge-groove (1 μm width, 1 μm height, and 1 μm spacing) (Fig. 1b) or post (1 μm diameter, 1 μm height, and 1 μm spacing) (Fig. 1c) were successfully templated into the thin-film scaffolds. Ridge-groove topography is a common feature used to align and elongate cells, whereas post-topography prevents cell spreading.

### *Cell proliferation on PCL scaffolds*

After seeding $2 \times 10^5$ $GFP^+$ mRPCs on each topography of the PCL scaffold, approximate 10% of the cells remained adhered at day 1, as revealed by averaged GFP intensities. The adherent cell number at day 1 steadily increased through day 7. At day 3, the cell number doubled and at day 7, the number had a 3.5-time increase (Fig. 1j). At day 7, cluster was formed

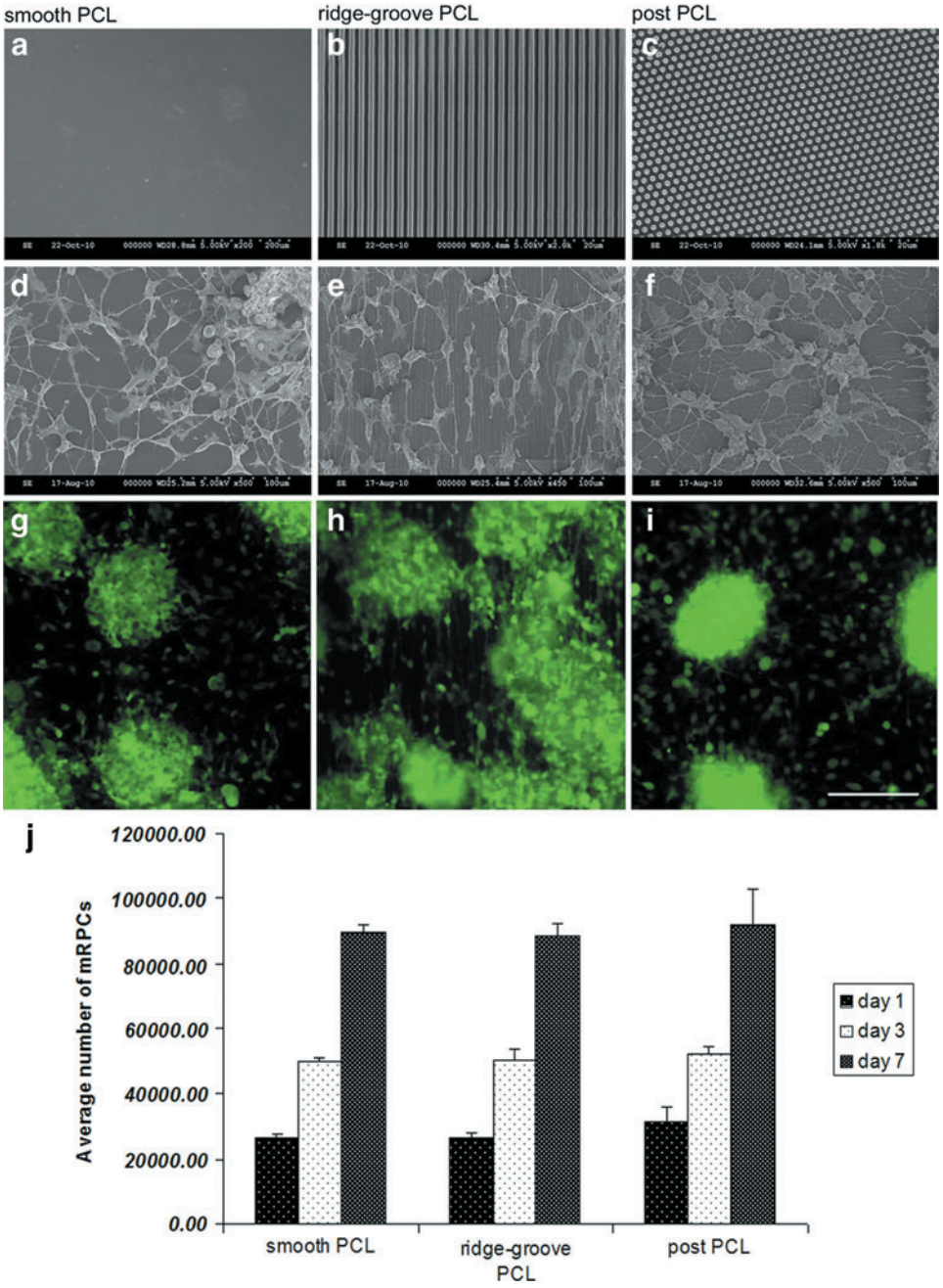


**FIG. 1.** Cell morphology and proliferation on PCL scaffolds. **(a–c)** SEM of the PCL scaffolds without cells. **(d–f)** The morphology of mRPCs grown on the corresponding PCL scaffolds for 7 days. **(g–i)** Fluorescent micrographs of mRPCs on the corresponding PCL scaffolds 7 days after plating. (GFP, *green*) **(j)** The average cell number of mRPCs cultured on different topographies of PCL scaffolds was calculated at day 1, 3, and 7. Scale bar: 250 μm. mRPC, mouse retinal progenitor cell; PCL, polycaprolactone; SEM, scanning electron microscope. Color images available online at www.liebertpub.com/tea

across each topography, and some single cells attached to the surface of the PCL scaffolds and spread processes (Fig. 1g–i). It seemed that mRPC proliferation pattern on different topographies of the PCL scaffolds was similar.

### *Cell differentiation on different substrates*

Mechanical stiffness and topography are two important mechanical cues responsible for cell morphologic adaptations and subsequent changes in protein and gene expression levels.[21] To elucidate which factor is more important for cellular differentiation, different topographies of PCL scaffolds with similar stiffness and two other substrates (glass and polystyrene) with different stiffness were used in this study.

Morphological changes are generally the first indicator of cell differentiation. Therefore, SEM was utilized to examine cell morphological changes in response to the topography. Morphological changes were characterized in terms of cell area, elongation, and alignment. Elongation is calculated by (major axis − minor axis)/(major axis + minor axis), a circular cell would have an elongation of 0. Alignment was calculated by measuring the angle between the cell's major axis with the direction of the ridge-grove, or the horizontal X-axis for the post-topography and control substrates. Unlike the previous study,[9] mRPCs grown on microfabricated PCL scaffolds not only formed clusters, but also spread fan-like processes out to neighboring cells (Fig. 1d–f). No statistical difference was apparent across topographies in terms of cell area. Cells cultured on the smooth PCL scaffolds

were shown to have random alignment (52.2°), little elongation (0.48) (Fig. 1d). mRPCs cultured on post-PCL scaffolds were found to have random alignment (50.4°) and a more circular cell morphology (0.28) (Fig. 1f). The most pronounced morphological changes occurred in mRPCs cultured on ridge-groove PCL scaffolds, and these changes could be seen as early as 3 days postplating. These cells were found to align (9.5°) and elongate (0.57) in the direction of ridge-groove surfaces (Fig. 1e). The morphology of cells cultured on glass was as similar as that grown on smooth PCL scaffolds (data not shown).

Compared to cells cultured on glass, a higher percentage of mRPCs grown on PCL scaffolds expressed photoreceptor markers crx (early photoreceptor marker), recoverin (calcium-binding protein, photoreceptor marker), and rhodopsin (G-protein-coupled receptor, rod photoreceptor marker) (Fig. 2a). Some rhodopsin-positive cells spread long processes, which appeared to resemble inner or outer segment (Fig. 2a, arrow head indicating the process of the same cell in low magnification [above] and high magnification [below], separatively). To demonstrate whether crx staining was nuclear, crx and DAPI were stained simultaneously (Fig. 2b). A significant increase ($p < 0.001$) of crx, recoverin, and rhodopsin-positive cells was detected in mRPCs grown on PCL scaffolds compared to glass (Fig. 2c). However, no significant differences were detected between different topographies of PCL scaffolds.

Corresponding to the ICC results, western blot and RT-PCR analysis revealed higher protein (Fig. 3a, b) and gene (Fig. 3c, d) expression levels of photoreceptor markers in cells grown on PCL scaffolds compared with those on glass. We further investigated the different levels of these markers between different topographies. The protein expression level of crx, recoverin, and rhodopsin between different topographies was significantly different, except that of recoverin between smooth and ridge-groove PCL scaffolds, and rhodopsin between smooth and ridge-groove PCL scaffolds. As for the gene expression levels, except those of crx between ridge-groove and post-PCL scaffolds, and rhodopsin between smooth and post-PCL scaffolds, the differences of these markers between different topographies were significant. The protein expression level of crx in smooth PCL scaffolds and recoverin in post-PCL scaffolds was inconsistent with the gene expression level, which may be attributed to the decreased translation and consequent stockpiling of mRNA.[22]

Although different topographies of these PCL scaffolds induced morphological adaptation, and subsequent protein and gene changes, it appeared that some other factors of these thin-film PCL scaffolds were more important in directing mRPCs toward a photoreceptor fate. Stiffness was a possible factor and has been shown to influence differentiation. As glass is not only stiffer, but also thicker and less modifiable than the PCL scaffold, we then constructed a 5-μm-thin polystyrene to further investigate the role of stiffness on cell differentiation. It demonstrated that lower gene expression level of the photoreceptor markers was seen on cells grown on polystyrene than those grown on glass (Fig. 3e, f). ICC and western blotting were conducted and the results showed that the protein expression patterns of mRPCs grown on polystyrene were similar to those grown on glass (data not shown).

We further observed the behavior of human RPCs on PCL scaffolds. After 7-day plating, the subpopulation of human RPCs obtained the expression of photoreceptor markers, such as recoverin (Fig. 4a), rhodopsin (Fig. 4b), and ROM1 (Fig. 4c). However, rhodopsin and ROM1 were not detected in cells plating on glass or before plating on PCL scaffolds (data not shown). The gene expression of these photoreceptor markers (Fig. 4d) was almost corresponding to the ICC results.

### *Calcium imaging*

Calcium imaging was also performed to evaluate neuronal properties between substrates. Using Fura-2-loaded mRPCs, the ratio of Δ 340/380 nm fluorescence indicated changes in intracellular calcium levels. Analysis of baseline Fura-2 signal between mRPCs grown on PCL scaffolds and glass showed higher Fura-2 levels of mRPCs cultured on PCL scaffolds than those grown on glass ($n = 4$). Both smooth and post-PCL scaffolds showed significant increases above glass (Fig. 3g). Evaluation of the time course of mRPCs cultured on each substrate revealed comparable responses to 1 mM glutamate exposure (Fig. 3h). Analysis of peak amplitude responses to 1 mM glutamate across conditions showed increases in Fura signal for mRPCs cultured on ridge-groove and post-PCL scaffolds compared to glass (Fig. 3i). Here, amplitude and duration of mRPC response to stimulation were observed as a measure of functional maturation.

### *Explant cultures*

Our *in vitro* results showed that ridge-groove PCL scaffolds were able to induce evident morphologic adaptations of mRPCs and upregulation of photoreceptor markers, which appeared to be optimal for rhodopsin expression. To investigate the restorative capacity of these mRPC/PCL scaffold constructs, we chose ridge-groove PCL scaffolds for the following studies.

After 7 days of coculturing mRPC/PCL scaffold constructs with explants from $Rho^{-/-}$ mice, cells from these scaffold constructs migrated extensively and took up residence in all retinal layers. Compared to single cells, mRPCs delivered via PCL scaffolds achieved better integration and more cells integrated into both the outer nuclear layer (ONL) and the inner nuclear layer (INL) (Fig. 5a–c). Cells still preferred the INL as previously reported,[3,20] but the average number of the integrated cells in the ONL was higher when cells were delivered via PCL scaffolds (Fig. 5c). Cells that integrated into the remaining ONL could express recoverin (Fig. 5h). More recoverin and rhodopsin-positive cells were observed when cells were delivered via PCL scaffolds than single cells (Fig. 5l). Some cells were able to make contact with residual PKC-positive cells (Fig. 5f), and some were able to express the synapse marker synaptophysin (Fig. 5g). Interestingly, a few cells were positive for crx (Fig. 5d) and the cone marker s-opsin (Fig. 5e).

Rhodopsin is an important element of the phototransduction cascade and essential for visual function. In our previous study, rhodopsin-positive cells were not detected in $Rho^{-/-}$ mice whether mRPCs were transplanted alone or co-transplanted with MMP2 microspheres.[20] In this study, rhodopsin-positive cells were still not observed when

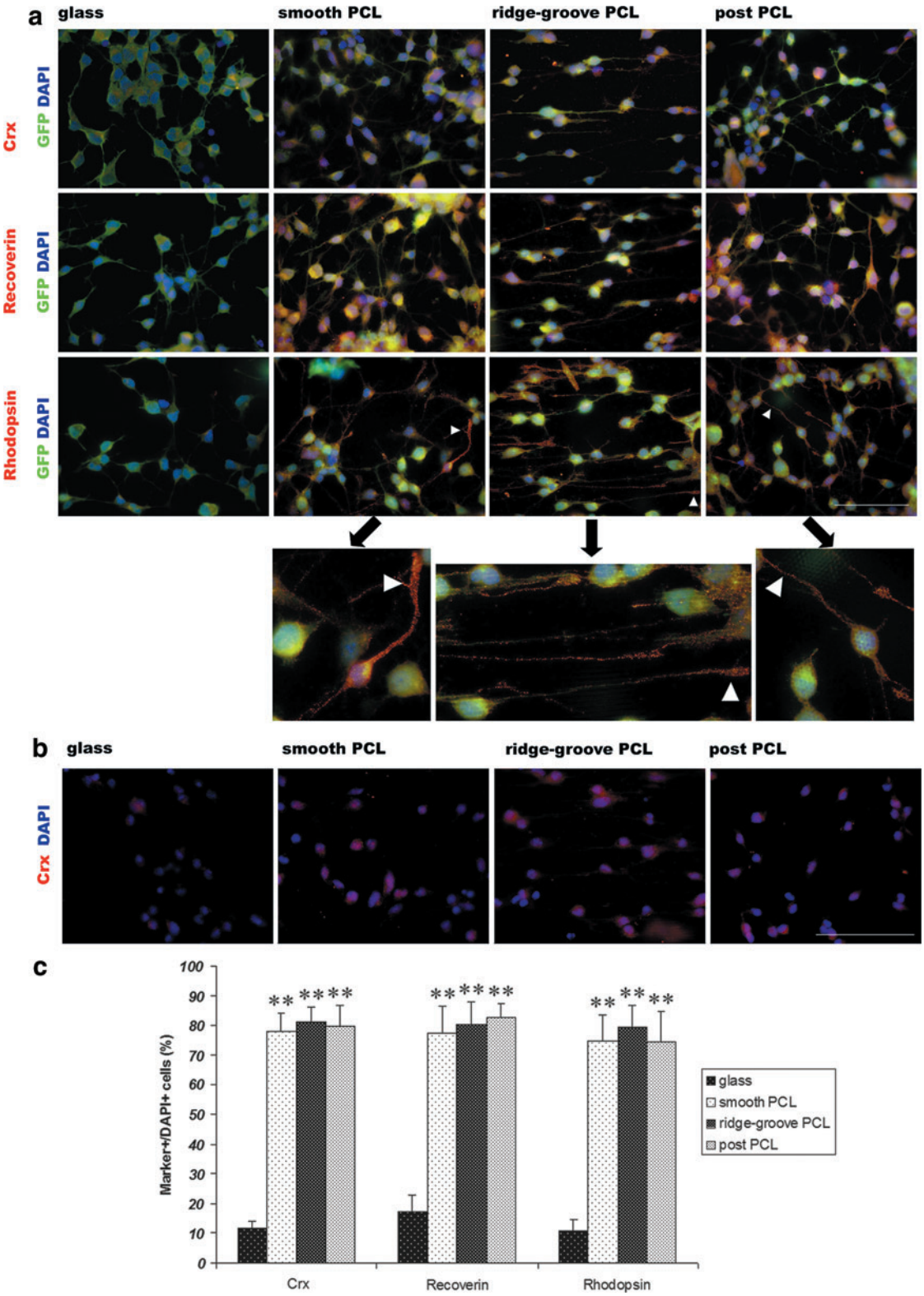


**FIG. 2.** Immunocytochemistry of mRPCs grown on PCL scaffolds and glass. **(a)** Differentiation of mRPCs on PCL scaffolds and glass for 7 days. *Arrow head* indicated the process of a rhodopsin-positive cell. The images below the *arrows* were the corresponding ones of high magnification. **(b)** Crx staining of mRPCs on PCL scaffolds and glass for 7 days. **(c)** The percentage of crx, recoverin, and rhodopsin-positive cells to DAPI. The differences of these positive cells between PCL scaffolds and glass were significant. Scale bar: 100 μm. $^{**}p < 0.001$. DAPI, 4′,6′-diamidino-2-phenylindole hydrochloride. Color images available online at www.liebertpub.com/tea

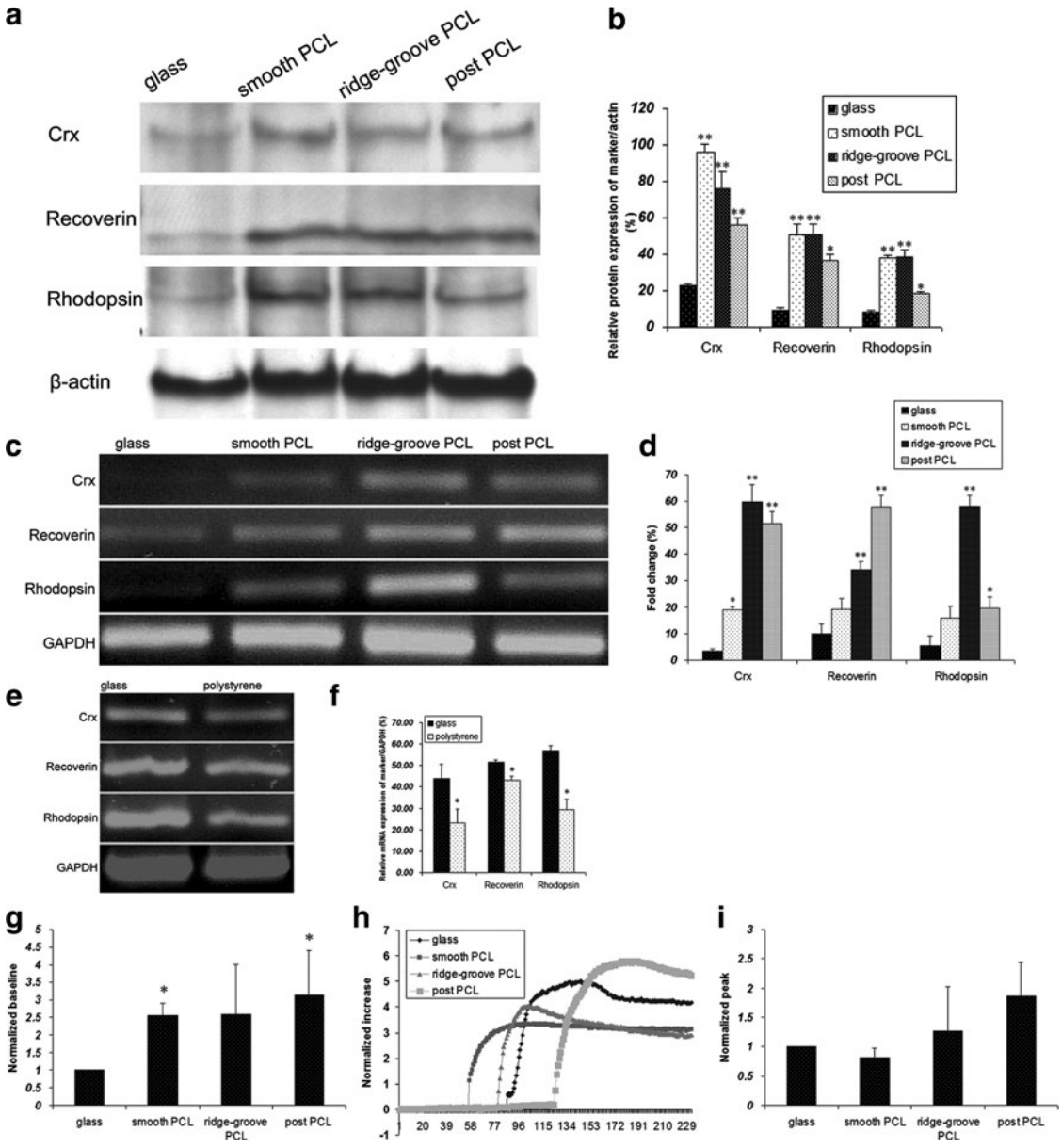


**FIG. 3.** Protein expression, gene expression, and calcium imaging of mRPCs grown on PCL scaffolds and glass. **(a, b)** The protein expression of three photoreceptor markers in cells grown on PCL scaffolds and glass. Higher protein expression of these photoreceptor markers was detected in cells grown on PCL scaffolds than those grown on glass. **(c, d)** The gene expression of three photoreceptor markers in cells grown on PCL scaffolds and glass. Compared to those grown on glass, higher gene expression of these photoreceptor markers was detected in cells grown on PCL scaffolds. **(e, f)** Comparison of the gene expression of three photoreceptor markers between cells grown on glass and polystyrene. **(g-i)** Fura-2 values were analyzed between mRPCs grown on PCL scaffolds and glass. **(g)** Baseline $Ca^{2+}$ levels. **(h)** Time course of mRPCs stimulated with 1 mM glutamate. **(i)** Peak response amplitudes to 1 mM glutamate. $*p < 0.05$, $**p < 0.001$.

coculturing single mRPCs with explants from $Rho^{-/-}$ mice (Fig. 5l). To test whether the complete absence of rhodopsin expression in $Rho^{-/-}$ hosts would affect the differentiation of the grafted cells, we put the mRPC/PCL scaffold construct onto $Rho^{-/-}$ and age-matched wild-type retinal explants. After 7-day coculture, both recoverin and rhodopsin-positive cells were detected in retinal explants (Fig. 5h–k). The numbers of recoverin-positive cells were similar in both types, but the number of rhodopsin-positive cells in $Rho^{-/-}$ mice was still lower than that in wild-type mice (Fig. 5m). The results suggested that predifferentiation of mRPCs on PCL scaffolds may overcome the inhibitive environment for cellular differentiation.

### *Subretinal transplantation*

To evaluate the behavior of mRPC/PCL scaffold constructs *in vivo*, we transplanted them into the subretinal space of $Rho^{-/-}$ mice and retinal samples were collected 3 weeks after transplantation. Using a retinal camera and SD-OCT, we could clearly see the scaffold construct located superiorly to the optic disc with the retinal vessels sitting on

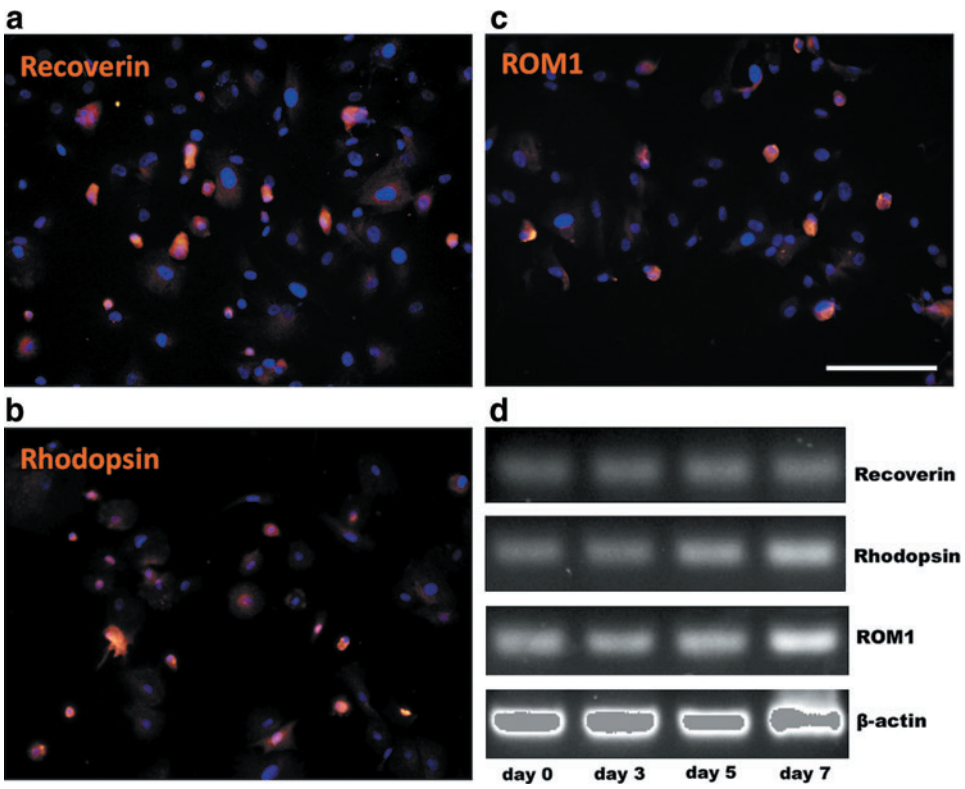


**FIG. 4.** Immunocytochemistry and gene expression of human RPCs on PCL scaffolds. Human RPCs showed polarized expression of recoverin **(a)**, rhodopsin **(b)**, and ROM1 **(c)** after 7 days of differentiation **(d)**. The gene expression of three photoreceptor marks in cells grown on PCL scaffolds over 7 days of differentiation. Scale bar: 100 μm. ROM1, rod outer membrane 1. Color images available online at www.liebertpub.com/tea

its surface (Fig. 6a, b). The scaffold construct was flat and no evident disturbance of the host retina was detected (Fig. 6c). Some cells stayed attached to the PCL scaffolds after transplantation and some began to migrate into the host retina (Fig. 6d). Cells that integrated into the residual ONL could express rhodopsin (Fig. 6e). Recoverin-positive cells were also found in the ONL. Some recoverin-positive cells made contact with residual PKC-positive cells (Fig. 6f–k), and some expressed the synapse marker synaptophysin (Fig. 6l–q).

## Discussion

Cell transplantation is a promising strategy for retinal repair in patients with RP and AMD. To achieve clinical relevance, more efficient cellular delivery and enhanced photoreceptor differentiation are needed. In this study, we developed a novel biodegradable thin-film PCL scaffold with varying topographies. The PCL scaffold alone appeared to have the potential to direct mRPCs toward a photoreceptor fate *in vitro* and subsequently was able to be used as a vehicle to deliver cells into the host retina, contributing to the rebuilding of complex and finely structured tissues of the outer retina.

Previous studies suggest that delivery of photoreceptor precursors and photoreceptor-committed cells may facilitate differentiation toward photoreceptors.[4, 14–16] Limited transplantable cell sources of photoreceptor precursors remains an obstacle in developing practical transplantation therapies. *In vitro* expansion of proliferating donor cells and then directing them toward photoreceptor-committed cells have the potential to overcome this problem. Previously we have shown that both mouse and human RPCs may be isolated from the developing retina and expanded *in vitro* with the preserved ability to make photoreceptors.[18] Conventional methods to induce differentiation use biochemical agents, such as chemicals, cytokines and growth factors.[14,23] However, most of these factors are of animal origin. In addition, they are expensive, and it is difficult to choose the ideal concentration for efficient differentiation without unintended effects. In this study, the PCL scaffold was developed and used as a substrate to induce cellular differentiation. To exclude the effect of other agents on cell differentiation, all the scaffolds were only treated with oxygen plasma, which was widely used to enhance cell adhesion.[24–26] Laminin and induction agents were not added for mRPCs, but fibronectin was added for human RPCs. Our results demonstrated that the PCL scaffold with nano-topographies could interact with mRPCs and human RPCs, and it had the potential to direct these cells toward a photoreceptor fate, thus providing the possibility to be used as a platform to differentiate cells before transplantation, which may facilitate the desired outcome while simultaneously inhibiting undesirable proliferation and differentiation.

Increasing studies indicate that besides chemical signals, mechanical tension-dependent changes in cell shape and cytoskeletal structure are critical for control of growth, and directing cell fate.[27] Topography has been demonstrated to induce cellular differentiation by directing cell morphologic adaptations and subsequent changes in protein and gene expression levels.[10,28–31] With the development of material science, it is feasible to tailor spatial control over topography with independent control of feature size and shape, thus providing a precise, rapid, inexpensive, and reproducible method to create polymer scaffolds with different topographies. These micropatterned substrates can be designed

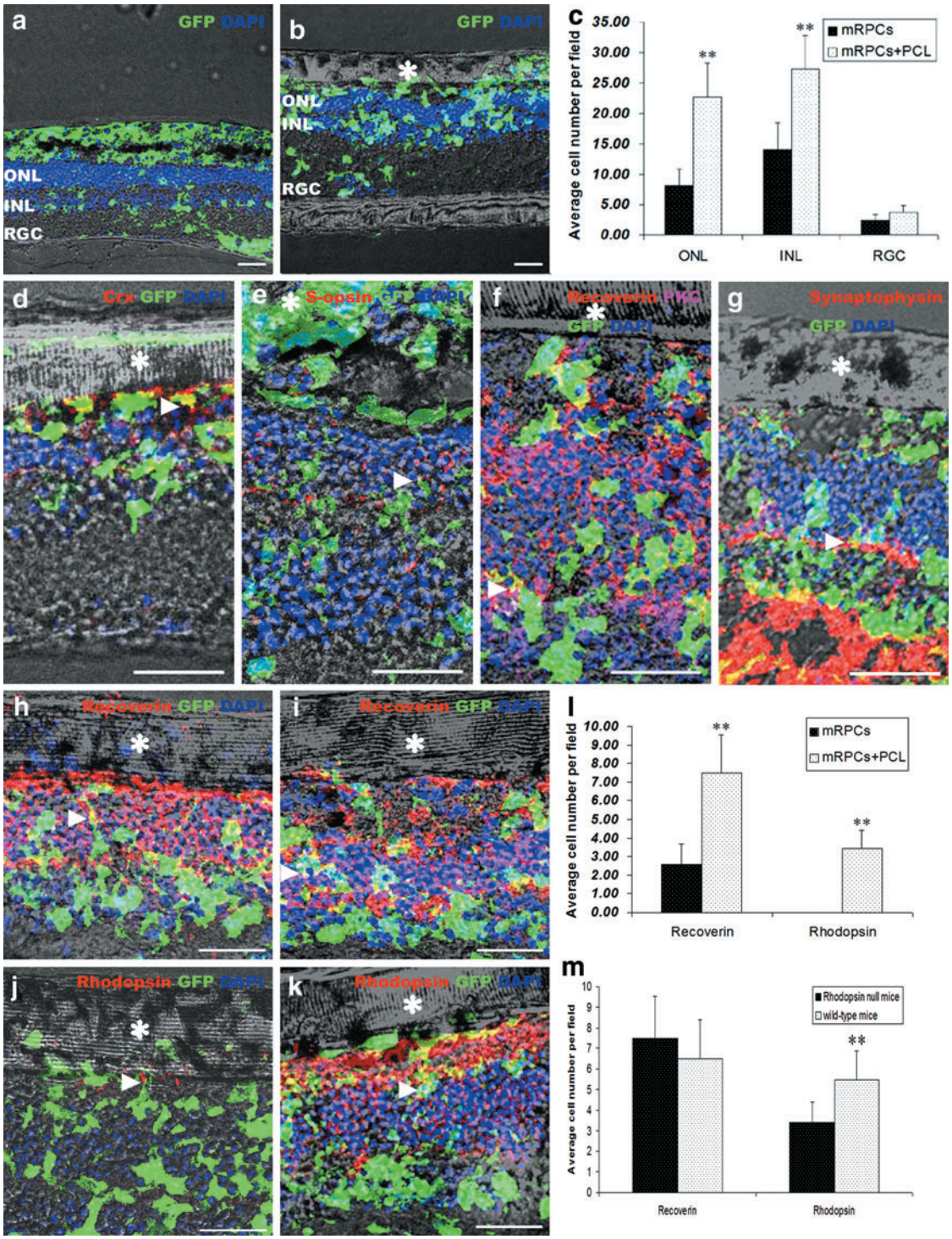


**FIG. 5.** Delivery of mRPC/PCL scaffold constructs to retinal explants. Retinal explants from $Rho^{-/-}$ **(a, b, d–h, j)** and wild-type mice **(i, k)** were cocultured with the ridge-groove mRPC/PCL scaffold constructs **(b, d–k)** or single cells **(a)** for 7 days and then collected for immunochemistry **(d–k)**. **(a, b)** Fluorescent images of mRPCs cocultured with retinal explants. **(c)** The average number of $GFP^+$ cells that migrated into different layers of the host retina. **(l)** The average number of integrated recoverin and rhodopsin-positive cells when delivering via PCL scaffolds or single cells. **(m)** Comparison of the average number of integrated recoverin and rhodopsin-positive cells between $Rho^{-/-}$ mice and wild-type mice. * Indicates the ridge-groove PCL scaffold. *Arrow head* indicates the crx **(d)**, s-opsin **(e)**, recoverin **(h, i)**, and rhodopsin **(j, k)**-positive cells, the contact between the recoverin-positive cell and the residual PKC-positive cell **(f)**, the synaptophysin-positive synapse **(g)**. $GFP^+$, green fluorescent protein positive; INL, inner nuclear layer; ONL, outer nuclear layer; PKC, protein kinase C; RGC, retinal ganglion cell. Scale bar: 30 μm. $^{**}p < 0.001$. Color images available online at www.liebertpub.com/tea

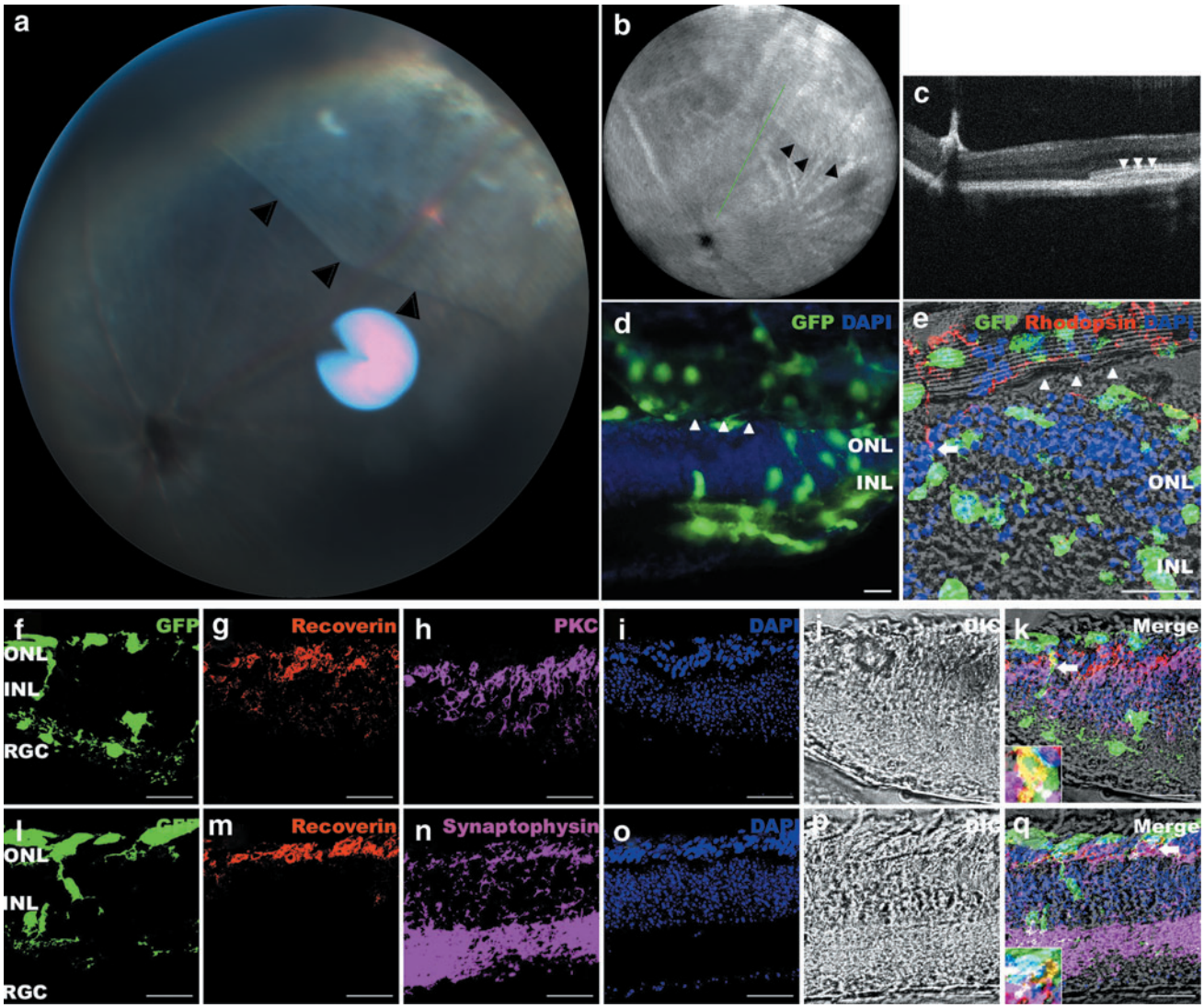


**FIG. 6.** Transplantation of mRPC/PCL scaffold constructs into the subretinal space of $Rho^{-/-}$ mice. **(a-c)** The same eye transplanted with the mRPC/PCL scaffold construct. Retinal picture **(a)** and SD-OCT **(b, c)** were examined 1 week after transplantation. **(b)**: The fundus picture with indicated orientation of cross-sectional SD-OCT scan. The scanning line was shown in *green*. **(c)**: The corresponding B-scan at the implantation site of the construct to **(b)**. **(d–q)** Representative images of the samples collected 3 weeks after transplantation. **(d)** Three weeks after transplantation, cells migrated to different layers of the host retina. **(e)** An integrated rhodopsin-positive cell spread process (*arrow*). **(f–k)** An integrated recoverin-positive cell made contact with the residual PKC-positive cell (*arrow*, *inset*). **(l–q)** An integrated recoverin-positive cell expressed the synapse marker synaptophysin (*arrow*, *inset*). *Arrow head* indicated the PCL scaffold. Scale bar: 30 μm. SD-OCT, spectral domain optical coherence tomography. Color images available online at www.liebertpub.com/tea

to influence initial cell attachment and spreading, and allow the maintenance of differentiated cell phenotype throughout culture. Surface topographic cues similar to endogenous extracellular matrix (ECM) can direct cell morphogenesis via cell surface contact.[9,30] It is suggested that the influence of surface topography on differentiation is via cell surface receptors that act as mechanochemical transducers, activating signal transduction pathways and ultimately modulating gene expression and protein expression.[29] In this study, we constructed the PCL scaffold with different topographies using microfabrication techniques and a templating process, which provided uniform and precise control of topography. Compared to other topographies, mRPCs cultured on the ridge-groove PCL scaffold showed substantial elongation and higher rhodopsin expression. The possible underlying mechanism might be due to the elongation of the cytoskeleton during changes in the morphology of cells guided by ridge-groove patterns, which resulted in a transfer of tensional force to the nuclei and then influenced gene expression and signal transduction.[25,32–34]

Mechanical stiffness is also an important factor responsible for cellular growth and differentiation.[35] Cells preferentially differentiate into distinct cell types when cultured on ECM with a mechanical stiffness that is most similar to that of the respective *in vivo* tissue.[21] Cells tune their internal stiffness to match the compliance of their ECM via

nonmuscle myosin II. Myosin II is thought to act as a cellular mechanosensor to detect mechanical stiffness and in turn, influence cellular lineage specification by modulating actin polymerization and cross-linking. This response may be responsible for altering cell morphology and gene expression during tissue remodeling.[21,35–40] Recent studies have identified a range of 100–1000 Pa as being the optimal stiffness for neurogenic cell differentiation.[21,41] Neural stem cells cultured on these ''soft'' matrices ($<1000$ Pa) have been shown to develop neural morphology and express various neural markers.[41] However, it is confounding whether mechanical stiffness or topography is more important in cellular differentiation. Our study demonstrated that although topography appeared to be able to partially influence the morphology and expression patterns of the adhering mRPCs, mRPCs grown on these PCL scaffolds seemed to be more inclined to differentiate toward a photoreceptor fate than those grown on glass or polystyrene, regardless of different topographies. The differentiation of human RPCs on these PCL scaffolds showed similar results. Before these PCL scaffolds could be used as a feasible platform to induce cellular differentiation, more studies were needed, such as defining the stiffness of these PCL scaffolds, examining the differentiation of different cell types on these PCL scaffolds, elucidating the underlying mechanism and so on.

Since it is not feasible to isolate photoreceptor precursors in clinical application, we tried to predifferentiate RPCs toward photoreceptor-committed cells *in vitro* using the PCL scaffold. With this methodology, grafted cells from these PCL scaffolds were able to integrate into the ONL and express photoreceptor markers. The results from this study and others showed promising of this platform in clinical settings.[42,43] However, fewer rhodopsin-positive cells were detected in $Rho^{-/-}$ mice than wild-type mice. It may relate to the complete absence of rhodopsin expression in $Rho^{-/-}$ mice or the state of the grafted cells. It is suggested that these PCL scaffolds may trigger a trend in mRPCs toward a differentiated state rather than clear and stable evidence of terminal differentiation. Moreover, even after mRPCs have exited the mitotic cycle, they still retained a level of plasticity and could change expression patterns and redirect fate.[44,45] So it is important to define the state of these predifferentiated cells by comparing them with photoreceptor precursors and look for ways for stable differentiation. Recent studies showed that γ-secretase inhibitor N-[N-(3,5-difluorophenacetyl-L-alanyl)]-S-phenylglycine t-butyl ester (DAPT) significantly increased the proportion of crx-positive photoreceptor precursors, suppressed expression of differentiation inhibitors hes1 and hes5 and inhibited proliferation.[5,46] Fabrication with DAPT or other induction factors that could direct cells toward stable photoreceptor-committed cells in these PCL scaffolds may become a useful direction for retinal regeneration.

In conclusion, we constructed a novel biodegradable thin-film PCL scaffold with different nano-topographies. Compared with control substrates, these PCL scaffolds showed enhanced potential to organize and differentiate mRPCs toward photoreceptor-committed cells *in vitro.* When delivering these mRPC/PCL scaffold constructs to the retinal explants or the subretinal space, cells were capable of integrating into the ONL and expressing photoreceptor markers. Although the underlying mechanism of these PCL scaffolds on cellular differentiation is unclear, these PCL scaffolds provide a promising strategy to address critical biological constraints related to retinal regeneration.

## Acknowledgments

We would like to thank Peter Humphries (Trinity College, Dublin) for providing $Rho^{-/-}$ mouse breeding pairs, D.F. Chen (Harvard Medical School) for helpful suggestions, and D. Pottle, S. Qi, M. Saint-Geniez, K.S. Cho (Harvard Medical School) for technical assistance. Financial support was provided by the Lincy Fundation Discovery Eye Foundation, Grousbeck Foundation (Cep290 Consortium).

## Disclosure Statement

No competing financial interests exist.

## References

1. Jager, R.D., Mieler, W.F., and Miller, J.W. Age-related macular degeneration. N Engl J Med **358,** 2606, 2008.
2. Sahel, J., Bonnel, S., Mrejen S., and Paques, M. Retinitis pigmentosa and other dystrophies. Dev Ophthalmol **47,** 160, 2010.
3. Klassen, H.J., Ng, T.F., Kurimoto, Y., Kirov, I., Shatos, M., Coffey, P., and Young, M.J. Multipotent retinal progenitors express developmental markers, differentiate into retinal neurons, and preserve light-mediated behavior. Invest Ophthalmol Vis Sci **45,** 4167, 2004.
4. Lamba, D.A., Gust, J., and Reh, T.A. Transplantation of human embryonic stem cell-derived photoreceptors restores some visual function in Crx-deficient mice. Cell Stem Cell **4,** 73, 2009.
5. Osakada, F., Ikeda, H., Mandai, M., Wataya, T., Watanabe, K., Yoshimura, N., *et al.* Toward the generation of rod and cone photoreceptors from mouse, monkey and human embryonic stem cells. Nat Biotechnol **26,** 215, 2008.
6. Lavik, E.B., Klassen, H., Warfvinge, K., Langer, R., and Young, M.J. Fabrication of degradable polymer scaffolds to direct the integration and differentiation of retinal progenitors. Biomaterials **26,** 3187, 2005.
7. Neeley, W.L., Redenti, S., Klassen, H., Tao, S., Desai, T., Young, M.J., *et al.* A microfabricated scaffold for retinal progenitor cell grafting. Biomaterials **29,** 418, 2008.
8. Redenti, S., Neeley, W.L., Rompani, S., Saigal, S., Yang, J., Klassen, H., *et al.* Engineering retinal progenitor cell and scrollable poly(glycerol-sebacate) composites for expansion and subretinal transplantation. Biomaterials **30,** 3405, 2009.
9. Redenti, S., Tao, S., Yang, J., Gu, P., Klassen, H., Saigal, S., *et al.* Retinal tissue engineering using mouse retinal progenitor cells and a novel biodegradable, thin-film poly(e-caprolactone) nanowire scaffold. J Ocul Biol Dis Infor **1,** 19, 2008.
10. Steedman, M.R., Tao, S.L., Klassen, H., and Desai, T.A. Enhanced differentiation of retinal progenitor cells using microfabricated topographical cues. Biomed Microdevices **12,** 363, 2010.
11. Tao, S., Young, C., Redenti, S., Zhang, Y., Klassen, H., Desai, T., *et al.* Survival, migration and differentiation of retinal progenitor cells transplanted on micro-machined poly(methyl methacrylate) scaffolds to the subretinal space. Lab Chip **7,** 695, 2007.

12. Tomita, M., Lavik, E., Klassen, H., Zahir, T., Langer, R., and Young, M.J. Biodegradable polymer composite grafts promote the survival and differentiation of retinal progenitor cells. Stem Cells **23,** 1579, 2005.
13. Tucker, B.A., Redenti, S.M., Jiang, C., Swift, J.S., Klassen, H.J., Smith, M.E., *et al.* The use of progenitor cell/biodegradable MMP2-PLGA polymer constructs to enhance cellular integration and retinal repopulation. Biomaterials **31,** 9, 2009.
14. Hirami, Y., Osakada, F., Takahashi, K., Okita, K., Yamanaka, S., Ikeda, H., *et al.* Generation of retinal cells from mouse and human induced pluripotent stem cells. Neurosci Lett **458,** 126, 2009.
15. MacLaren, R.E., Pearson, R.A., MacNeil, A., Douglas, R.H., Salt, T.E., Akimoto, M., *et al.* Retinal repair by transplantation of photoreceptor precursors. Nature **444,** 203, 2006.
16. Tucker, B.A., Park, I.H., Qi, S.D., Klassen, H.J., Jiang, C., Yao, J., *et al.* Transplantation of adult mouse iPS cell-derived photoreceptor precursors restores retinal structure and function in degenerative mice. PLoS One **6,** e18992, 2011.
17. Ryskamp, D.A., Witkovsky, P., Barabas, P., Huang, W., Koehler, C., Akimov. N.P., *et al.* The polymodal ion channel transient receptor potential vanilloid 4 modulates calcium flux, spiking rate, and apoptosis of mouse retinal ganglion cells. J Neurosci **31,** 7089, 2011.
18. Baranov, P.Y., Tucker, B.A., and Young, M.J. Low-oxygen culture conditions extend the multipotent properties of human retinal progenitor cells. Tissue Eng Part A **20,** 1465, 2014.
19. Ogilvie, J.M., Speck, J.D., Lett, J.M., and Fleming, T.T. A reliable method for organ culture of neonatal mouse retina with long-term survival. J Neurosci Methods **87,** 57, 1999.
20. Yao, J., Tucker, B.A., Zhang, X., Checa-Casalenqua, P., Herrero-Vanrell, R., and Young, M.J. Robust cell integration from co-transplantation of biodegradable MMP2-PLGA microspheres with retinal progenitor cells. Biomaterials **32,** 1041, 2011.
21. Engler, A.J., Sen, S., Sweeney, H.L., and Discher, D.E. Matrix elasticity directs stem cell lineage specification. Cell **126,** 677, 2006.
22. Krichevsky, A.M., and Kosik, K.S. Neuronal RNA granules: a link between RNA localization and stimulation-dependent translation. Neuron **32,** 683, 2001.
23. Lamba, D.A., Karl, M.O., Ware, C.B., and Reh, T.A. Efficient generation of retinal progenitor cells from human embryonic stem cells. Proc Natl Acad Sci U S A **103,** 12769, 2006.
24. He, W., Ma, Z., Yong, T., Teo, W.E., and Ramakrishna, S. Fabrication of collagen-coated biodegradable polymer nanofiber mesh and its potential for endothelial cells growth. Biomaterials **26,** 7606, 2005.
25. Lee, M.R., Kwon, K.W., Jung, H., Kim, H.N., Suh, K.Y., Kim, K., *et al.* Direct differentiation of human embryonic stem cells into selective neurons on nanoscale ridge/groove pattern arrays. Biomaterials **31,** 4360, 2010.
26. Wan, Y., Yang, J., Bei, J., and Wang, S. Cell adhesion on gaseous plasma modified poly-(L-lactide) surface under shear stress field. Biomaterials **24,** 3757, 2003.
27. Mammoto, A., and Ingber, D.E. Cytoskeletal control of growth and cell fate switching. Curr Opin Cell Biol **21,** 864, 2009.
28. Andersson, A.S., Backhed, F., von Euler, A., Richter-Dahlfors, A., Sutherland, D., and Kasemo, B. Nanoscale features influence epithelial cell morphology and cytokine production. Biomaterials **24,** 3427, 2003.
29. Flemming, R.G., Murphy, C.J., Abrams, G.A., Goodman, S.L., and Nealey, P.F. Effects of synthetic micro- and nano-structured surfaces on cell behavior. Biomaterials **20,** 573, 1999.
30. Foley, J.D., Grunwald, E.W., Nealey, P.F., and Murphy, C.J. Cooperative modulation of neuritogenesis by PC12 cells by topography and nerve growth factor. Biomaterials **26,** 3639, 2005.
31. Recknor, J.B., Sakaguchi, D.S., and Mallapragada, S.K. Directed growth and selective differentiation of neural progenitor cells on micropatterned polymer substrates. Biomaterials **27,** 4098, 2006.
32. Chen, C.S., Tan, J., and Tien, J. Mechanotransduction at cell-matrix and cell-cell contacts. Annu Rev Biomed Eng **6,** 275, 2004.
33. Jaalouk, D.E., and Lammerding, J. Mechanotransduction gone awry. Nat Rev Mol Cell Biol **10,** 63, 2009.
34. Thomas, C.H., Collier, J.H., Sfeir, C.S., and Healy, K.E. Engineering gene expression and protein synthesis by modulation of nuclear shape. Proc Natl Acad Sci U S A **99,** 1972, 2002.
35. Discher, D.E., Janmey, P., and Wang, Y.L. Tissue cells feel and respond to the stiffness of their substrate. Science **310,** 1139, 2005.
36. Chowdhury, F., Na, S., Li, D., Poh, Y.C., Tanaka, T.S., Wang, F., *et al.* Material properties of the cell dictate stress-induced spreading and differentiation in embryonic stem cells. Nat Mater **9,** 82, 2010.
37. Engler, A.J., Griffin, M.A., Sen, S., Bönnemann, C.G., Sweeney, H.L., and Discher, D.E. Myotubes differentiate optimally on substrates with tissue-like stiffness: pathological implications for soft or stiff microenvironments. J Cell Biol **166,** 877, 2004.
38. Mammoto, A., Connor, K.M., Mammoto, T., Yung, C.W., Huh, D., Aderman, C.M., *et al.* A mechanosensitive transcriptional mechanism that controls angiogenesis. Nature **457,** 1103, 2009.
39. Solon, J., Levental, I., Sengupta, K., Georges, P.C., and Janmey, P.A. Fibroblast adaptation and stiffness matching to soft elastic substrates. Biophys J **93,** 4453, 2007.
40. Vogel, V., and Sheetz, M. Local force and geometry sensing regulate cell functions. Nat Rev Mol Cell Biol **7,** 265, 2006.
41. Saha, K., Keung, A.J., Irwin, E.F., Li, Y., Little, L., Schaffer, D.V., *et al.* Substrate modulus directs neural stem cell behavior. Biophys J **95,** 4426, 2008.
42. Caio, V.R., Petr, B., Ana, C., Chi, W.K., Sarah, T., and Michael, J.Y. Pre differentiated human retinal progenitor cells integrate and express mature markers on the host retina. Abstract presented at the *ARVO Annual Meeting*, Fort Lauderdale, FL, 2012. Abstract no. A593.
43. Lawley, E., Baranov, P., and Young, M. Hybrid vitronectin-mimicking polycaprolactone scaffolds for human retinal progenitor cell differentiation and transplantation. J Biomater Appl **29,** 894, 2015.
44. Belliveau, M.J., Young, T.L., and Cepko, C.L. Late retinal progenitor cells show intrinsic limitations in the production of cell types and the kinetics of opsin synthesis. J Neurosci **20,** 2247, 2000.

45. Trimarchi, J.M., Stadler, M.B., Roska, B., Billings, N., Sun, B., Bartch, B., *et al.* Molecular heterogeneity of developing retinal ganglion and amacrine cells revealed through single cell gene expression profiling. J Comp Neurol **502,** 1047, 2007.
46. Eiraku, M., Takata, N., Ishibashi, H., Kawada, M., Sakakura, E., Okuda, S., *et al.* Self-organizing optic-cup morphogenesis in three-dimensional culture. Nature **472,** 51, 2011.

Address correspondence to:
*Michael J. Young, PhD*
*Department of Ophthalmology*
*Schepens Eye Research Institute*
*Harvard Medical School*
*20 Staniford Street*
*Boston, MA 02114*

*E-mail:* mchael_young@meei.harvard.edu

*Received: November 25, 2013*
*Accepted: November 18, 2014*
*Online Publication Date: March 18, 2015*